Hard x-ray source for flash radiography based on a 2.5 kJ plasma focus

F. Di Lorenzo, V. Raspa, P. Knoblauch, A. Lazarte, C. Moreno, and A. Clausse

Citation: Journal of Applied Physics **102**, 033304 (2007); doi: 10.1063/1.2767829
View online: http://dx.doi.org/10.1063/1.2767829
View Table of Contents: http://scitation.aip.org/content/aip/journal/jap/102/3?ver=pdfcov
Published by the AIP Publishing

Hard x-ray source for flash radiography based on a 2.5 kJ plasma focus

F. Di Lorenzo, V. Raspa, P. Knoblauch, A. Lazarte, and C. Moreno[a)]
Departamento de Física, FCEyN, PLADEMA-CNEA, INFIP-CONICET, Universidad de Buenos Aires, Pab. 1, Ciudad Universitaria, Buenos Aires 1428, Argentina

A. Clausse
PLADEMA-CNEA, CONICET, Universidad Nacional del Centro, Campus Universitario, Paraje Arroyo Seco, Tandil 7000, Buenos Aires, Argentina

(Received 30 May 2007; accepted 26 June 2007; published online 14 August 2007)

A compact tabletop plasma focus suitable for hard x-ray imaging applications is presented. The hard x-ray emission was characterized by means of an effective energy analysis, based on images obtained with a single shot. The effective energy of the radiation was estimated to be around 83 keV from radiographic images of metallic pieces. Numerical calculations, based on validated codes, are presented to give a quantitative interpretation of the experimental results. Experimental demonstration of the suitability of this device for introspective imaging of metallic pieces is also given. © *2007 American Institute of Physics*. [DOI: 10.1063/1.2767829]

I. INTRODUCTION

Plasma focus (PF) is one of the most cost-effective small fusion devices, which operates by producing intense electrical discharges between a pair of coaxial cylindrical electrodes located in a low pressure chamber (0.5–20 mbars). The device acts as a plasma accelerator gun in which the Lorentz force drives a plasma sheath along the electrodes, making it to collapse at the symmetry axis forming a hot dense plasma focus. Intense pulses of electromagnetic radiation as well as electron and ion beams are emitted as a result of the focalization process. Fusion reactions can be obtained if deuterium or deuterium-tritium mixtures are used, with the consequent emission of fast neutrons.

Apart from fusion and fundamental research, efforts were undertaken to investigate various technological applications based on either, the emitted particles, or the radiated electromagnetic field. Within the latter, applications such as soft x-ray imaging of biological specimens[1–4] or small samples[5] and soft x-ray lithography or micromachining[6–11] were reported. Other important results were obtained using a PF as an x-ray backlighter for photon energies of about 1 keV;[12,13] tailoring the output efficiency in the 1.2–1.3 keV window,[14] or enhancing the Cu $K\alpha$ (Ref. 15) line emission from the focus region. Specifically on x-ray imaging, Hussain *et al.*[16] studied a 1.8 kJ, 20 kV PF concluding that the device was suitable for good contrast radiography. More recently, a substantial enhancement of a PF performance as x-ray source was accomplished by preionizing the breakdown region with depleted uranium.[17] In all of the above mentioned advances, achieved using relatively small PF facilities with operating voltages and stored energies up to 36 kV and 4.6 kJ, respectively, mainly the low region of the x-ray spectrum ($h\nu < 30$ keV) was exploited.

On the other hand, hard x rays generated by a compact 4.7 kJ, 30 kV PF operated in deuterium were used to obtain radiographic images of metallic objects either static[18–20] or in fast rotation[21] and its neutron emission was used for side on water detection.[19,20]

In order to fully take advantage of the mentioned potentials, a PF device should be designed properly, providing flexibility, easy operation and maintenance, and portability. In this article, a compact design 2.5 kJ, 30 kV PF specially designed to perform as a hard x-ray radiation source suitable for flash radiography of metallic pieces is presented. The device is experimentally and theoretically characterized, and the suitability of applications is evaluated.

II. DEVICE AND METHODOLOGY

The PF capacitor bank is formed by eight capacitors (0.7 μF each) connected in parallel surrounding both the spark gap and discharge chamber to provide a minimum inductance connection. The bank is charged up to 30 kV (2.5 kJ of stored energy), delivering a peak current of 350 kA to the discharge chamber in a quarter of period of $\sim$1.3 μs. The electrodes are coaxial and formed by a hollow high-conductivity oxygen-free copper anode (central electrode) and by a barred bronze cathode. The insulator is made of Pyrex glass. The electrode-insulator set is coaxially placed inside a cylindrical 1.5 l stainless-steel chamber and 3 mm thick walls. A sketch of the chamber design is shown in Fig. 1, and a comprehensive list of electrical and geometrical parameters is given in Table I.

The electrode-insulator base, made on polyamide 6, was designed to stand the high voltage spikes induced during the focalization. The thickness of the insulator wall was chosen to be 4 mm. Pyrex insulators having 2 mm thick walls were tested, but they did not last much more than a hundred of shots. Such thin insulators usually broke after a number of intense focalizations on which, presumably, the effects of dielectric fatigue were being accumulated on the glass. The insulator free length ensures that the breakdown condition always occurs on the right branch of Paschen curve for all of the operating pressures. This design criterion contributes to

[a)]Electronic mail: moreno@df.uba.ar

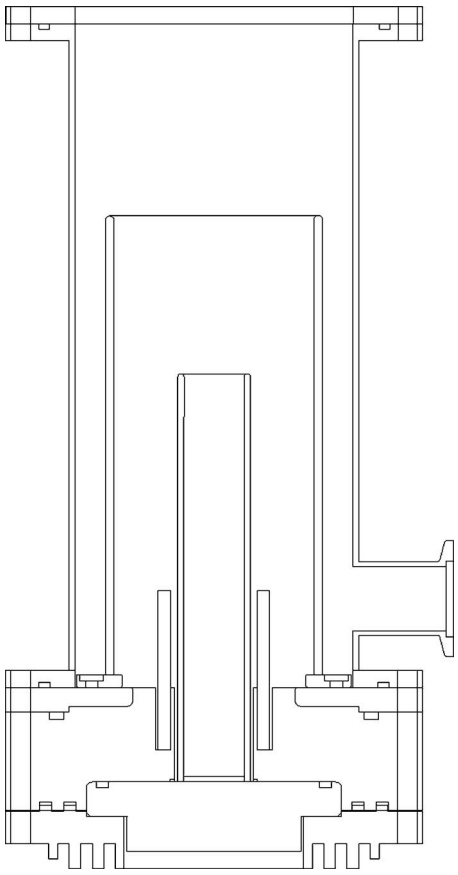

FIG. 1. Scketch of the chamber design (longitudinal cross section). The chamber walls, electrodes, and insulator can be seen along with the NW-25 vacuum connector.

TABLE I. Electrical and geometrical parameters of the device.

Footprint area (m^2)	0.25
Height (capacitor bank plus chamber) (m)	1
Control system height (m)	0.5
Volume (m^3)	~0.4
Weight (kg)	75
Capacity (μF)	5.6
Stray inductance (nH)	80
Resistance (mΩ)	20
Operation voltage (kV)	30
Stored energy at 30 kV (kJ)	2.5
Maximum current (kA)	350
Time to maximum current (μs)	~1.30
Filling gas pressure (mbars)	2–6
Filling gas	D_2
Anode material	Copper OFHC
Anode radius (mm)	12.5
Anode length (mm)	108
Cathode material	Bronze
Cathode radius (mm)	33.75
Cathode length (mm)	163
Insulator material	Pyrex glass
Insulator radius (mm)	19.25
Insulator free length (mm)	33.5
Insulator thickness (mm)	4.0

enhance the PF performance because the essential breakdown mechanisms are kept unchanged throughout the whole pressure range of interest. Figure 2 presents the Paschen curve measured on the actual device, for the actual electrode-insulator set showing the pressure operating region.

For ease of maintenance and operation, the device has only one triggerable high voltage switch, based on a presurized spark gap, which was constructed by modifying a Maxwell unit Model No. 40264, rated up to 100 kV, 100 kA. The modification consists in the addition of two extention rings to increase both the spark-gap chamber volume, and the inter-electrode superficial distance. These pieces, made on polyacetal, increased the spark-gap total height by 45 mm. They hold the central spark-gap plate (trigger electrode, made on brass) and go in the middle of the assembly (see Fig. 3). The two main electrodes, made also on brass, were correspondingly lengthened to keep the interelectrode gap length unchanged. Except for the main electrodes and the eight assembling screws (which also needed to be lengthened) the rest of the Maxwell original parts were used in the modified unit. Figure 4 shows a picture of the assembled switch.

The x-ray output was monitored using a photomultiplier tube optically coupled to a NE102A plastic scintillator. The assembly was placed 6.7 m away from the chamber, inside a Faraday cage to reduce noise pickup. The recorded signals show that the x-ray pulse duration is 50 ns full width at half maximum (FWHM), which are suitable for x-ray imaging of pieces in fast motion. Commercial AGFA Curix Ortho Regular cassette-film system was used together with standard developer and fixer recommended for that film. No special procedures other than those indicated by the manufacturer were required to process the films.

III. HXR SOURCE CHARACTERISTICS

A. Spatial location

At least two potential sources of hard x rays can be identified in PF discharges: the anode, against which accelerated electrons collide; and the focus itself, where unbounded electrons strongly interact with the ionic field of the

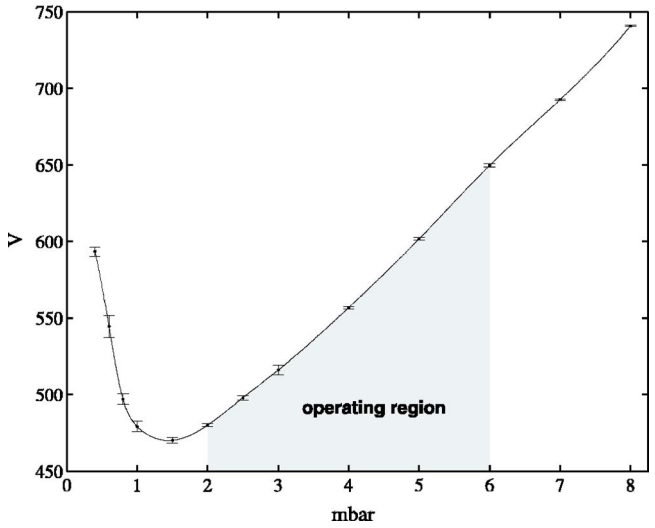

FIG. 2. Paschen curve for the plasma focus electrode-insulator set. Filling gas: deuterium.

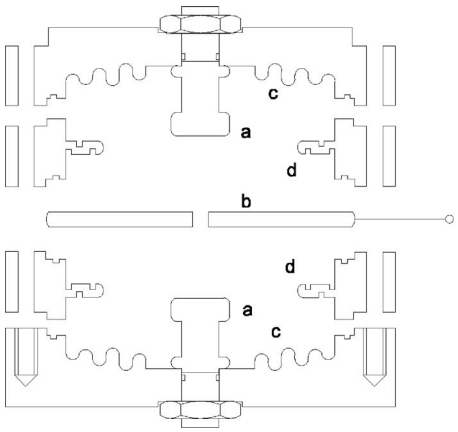

FIG. 3. Scketch of the spark-gap switch (diametral cross section): (a) main electrodes, (b) central electrode (trigger), (c) original polycarbonate case, and (d) polyacetal extentions.

dense plasma. While the characteristics of the former are similar to those of high voltage x-ray tubes, the x-ray spectrum emitted from the focus is softer.[22]

The anode bombardment, in turn, could take place in more than one location. In order to determine the spatial locations of the hard x-ray sources, successive radiographies were taken placing a radiographic film along the electrodes axis at different distances from the chamber top, up to 15 cm. Three of such film-chamber distances (X_i) are illustrated on Fig. 5. It was concluded that the radiation beam is collimated since the area of the radiographic films exposed to the radiation was found to depend on its distance to the discharge chamber, as can be seen on Fig. 5 (shaded regions).

The complete set of the analyzed radiographs clearly shows a dark circle image corresponding to the hard x-ray illuminated zone. X rays with energies below 30 keV are strongly attenuated ($\sim 10^9$ times) by the chamber front wall. Measuring the diameter of the irradiated area for several film-chamber distances, the distance from the source to the chamber top (Y) and the half aperture angle of the hard x-ray beam (α) were, respectively, calculated as (23.8 ± 3.5) cm and (0.24 ± 0.03) rad. The inferred spatial location is in agreement, within the experimental uncertainties, with a point source located at the bottom of the anode tube.

B. Effective energy

Since the spectrum of the emitted radiation is quite broad, it contains wavelengths far beyond the capability of the available spectrometers. Besides the pulse duration is so short that it prevents the use of single-event spectroscopy. Therefore, the spectrum was characterized by an efective average energy, defined as the energy that an equivalent monochromatic beam should have to experiment the same intensity attenuation. Assuming a continuous energy spectrum, the relative intensity attenuation due to a sample of thickness d is

$$\frac{I(d)}{I_0} = \frac{\int_0^\infty S(E) e^{-\mu(E)d} dE}{\int_0^\infty S(E) dE}, \tag{1}$$

where I_0 and $I(d)$ are the incident and transmitted intensities, respectively, $S(E)$ is the spectral density, E is the energy of the photons, and $\mu(E)$ is the linear attenuation coefficient for the filter material. As follows from its definition, the effective energy E^* is such that

$$\frac{I(d)}{I_0} = e^{-\mu(E^*)d}. \tag{2}$$

The magnitude $\mu(E^*)$ performs as an effective attenuation coefficient.

Measuring the attenuation ratio $I(d)/I_0$ for known sample thicknesses d of the same material, it is possible to estimate $\mu(E^*)$ for that material using Eq. (2). Once $\mu(E^*)$ is known, E^* can be estimated from the tabulated $\mu(E)$ relationship.

Several sets of metallic plates were imaged to study their relative absorption $I(d)/I_0$. The following metals and thicknesses were used as filters (± 0.02 mm): cadmium (1.10, 2.20, and 3.30 mm), copper (1.12, 2.24, 3.36, 4.48, and 5.60 mm), and nickel (1.60, 2.70, 4.30, and 5.40 mm). The film, together with the complete set of plates, was placed at (20.4 ± 0.02) cm from the chamber, and was irradiated with one shot. Figure 6 presents a digitized radiographic image of the filter set. The radiograph was obtained with a deuterium filling pressure of 3 mbars and a charging voltage of 30 kV. After digitizing the image, the relative intensity profile for each plate was obtained, corresponding to the attenuation dependence with the thickness and filter material. Thus, by comparing the corresponding gray tones of the digitized images, an estimation of the effective attenuation coefficient for each metal can be obtained.

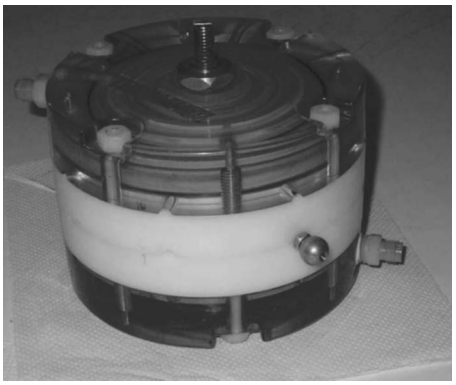

FIG. 4. Picture of the assembled spark gap.

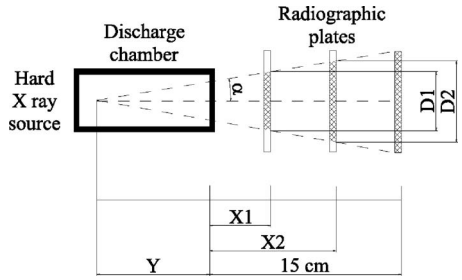

FIG. 5. Experimental setup to determine the spatial location of the hard x-ray source.

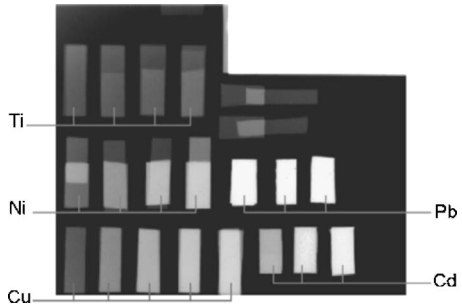

FIG. 6. Radiograph of the set of metallic filters employed to determine the effective energy of the hard x-ray radiation. Slabs of different thicknesses of each material were exposed, and their corresponding attenuations were compared. The lead filters were used as reference of total attenuation.

The effective attenuation coefficients obtained for cadmium, copper, and nickel are shown on Table II, along with their corresponding effective energies taken from Ref. 23. Even though the employed materials have absorption coefficients that differ significantly between each other, the obtained values for energy show good agreement with one another. All of them correspond to effective energies of (83 ± 10) keV.

To check if the film was not saturated, and if the gray level assignment by the digitizing process is proportional to the intensity reaching the film, it was verified that an exponential decay of the radiation intensity with the sample depth was obtained for each set of samples.

To verify that the measured effective energy is compatible with what can be expected for the voltage drop in the pinch V_p such voltage was estimated as

$$V_p = \frac{d(L_p I)}{dt}, \tag{3}$$

where I is the total current circulating through the pinch and L_p represents the pinch inductance, which in turn can be estimated as

$$L_p(t) = \frac{\mu_0 h(t)}{2\pi} \ln\left[\frac{r_e}{r(t)}\right], \tag{4}$$

where $h(t)$ and $r(t)$ are the pinch length and radius, respectively, and r_e represents the radius of the external electrode. The temporal dependence of $L_p(t)$ and $I(t)$ were evaluated resorting to the well known Lee model.[24]

Figure 7(a) shows the calculated temporal evolution of V_p considering a filling pressure of 3 mbars and a charging voltage of 30 kV. According to this model a voltage peak of approximately 110 kV can be expected during the focus, shortly before the maximum compression occurs. For this reason, a measured effective energy of 83 keV is considered to be compatible with what can be expected from a validated numerical code. Figure 7(b) shows the calculated pressure dependence of the maximum pinch voltage. For this particular device, it can be seen that the expected pinch voltage peak decreases with the filling pressure in the explored operation range.

TABLE II. Linear attenuation coefficients and effective energies measured for different metals.

Material	Attenuation factor (cm^{-1})	Effective energy (keV)
Cadmium	18.08	85±9
Copper	5.64	85±9
Nickel	6.68	80±8
Average effective energy		83±10

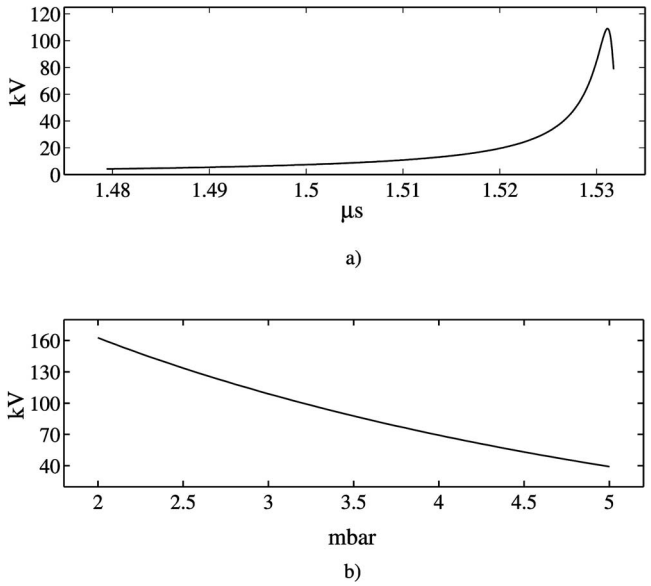

FIG. 7. (a) Calculated temporal evolution of the pinch voltage at 3 mbars of deuterium as filling gas and 30 kV of charging voltage. (b) Pressure dependence of the calculated maximum pinch voltage.

IV. RADIOGRAPHIC APPLICATIONS

The hard x-ray radiation output was used to obtain introspective images of metallic objects. Figure 8 shows a digitized radiograph of an aluminum climbing karabiner. The object was placed on the electrodes axis, outside the chamber, about 13 cm away from its front wall. The image has an overall spatial resolution of 1/50 mm (i.e., 50 pixels of the scanned image per millimeter measured on the object), limited by the digitizing process of the radiographic film. Submillimetric details of the internal mechanism can be easily distinguished, demonstrating the suitability of this PF device as a radiation source for introspective imaging of metallic objects. Although the geometric characteristics of the source itself are still to be determined, the degree of detail shown in Fig. 8 implies that the source size is well below the millimetric scale, since otherwise the images would not show sharp borders with such good contrast. This remains true even if three or four shots are superimposed on the same film; therefore, for radiographic purposes at least, the location of the hard x-ray source can be considered as presenting practically no variation from shot to shot.

V. CONCLUSIONS

A compact low energy plasma focus suitable for radiographic applications was presented and characterized as a hard x-ray radiation source. Radiographs of small metallic

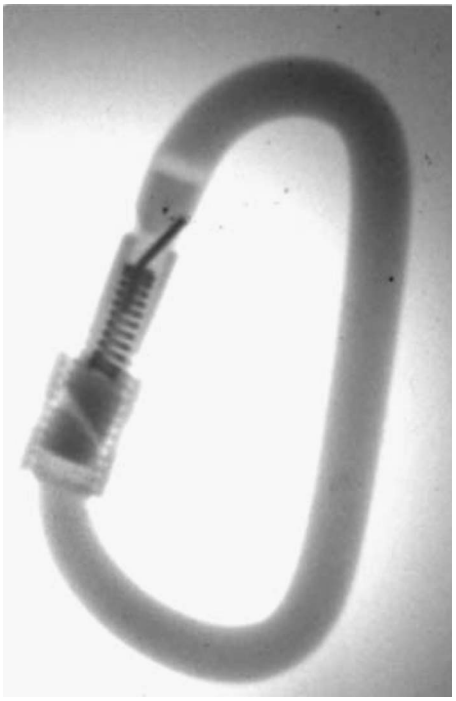

FIG. 8. Hard x-ray radiograph of an aluminum climbing karabiner obtained with one shot of the device. The object and radiographic plate were placed 13 cm away from the chamber top.

samples can be achieved in single shots, reaching an image spatial resolution of 20 μm per pixel of the scanned image. The spatial location of the radiation source was found to be placed on the anode base, and its position does not vary appreciably from shot to shot. The use of a hollow anode helps to collimate the output beam, which, in our case, has a 14° half aperture. An effective energy of the hard x-ray emissions of 83 keV was experimentally determined. This value is compatible with what can be expected from the pinch induced voltage evaluated using a validated numerical model.

ACKNOWLEDGMENTS

This research was supported by PLADEMA-CNEA, and Universidad de Buenos Aires. Four of the authors (F.D.L., A.L., V.R., and P.K.) are doctoral fellows of CONICET. Two of the authors (C.M. and A.C.) are members of CONICET.

[1] G. Decker and R. Wienecke, Physica B & C **82**, 155 (1976).
[2] F. Castillo-Mejía, M. Milanese, R. Moroso, J. Pouzo, and M. Santiago, IEEE Trans. Plasma Sci. **29**, 921 (2001).
[3] S. Hussain, S. Ahmad, M. Khan, M. Zakaullah, and A. Waheed, J. Fusion Energy **22**, 195 (2003).
[4] R. Rawat *et al.*, J. Fusion Energy **23**, 49 (2004).
[5] F. Castillo, J. Herrera, J. Rangel, A. Alfaro, M. Maza, V. Sakaguchi, G. Espinosa, and J. Golzarri, Braz. J. Phys. **32**, 3 (2002).
[6] Y. Kato and S. Be, Appl. Phys. Lett. **48**, 686 (1986).
[7] Y. Kato, I. Ochiai, Y. Watanabe, and S. Murayama, J. Vac. Sci. Technol. B **6**, 195 (1988).
[8] E. Bogolyubov *et al.*, Phys. Scr. **57**, 488 (1998).
[9] S. Lee, P. Lee, G. Zhang, X. Feng, V. Gribkov, M. Liu, A. Serban, and T. Wong, IEEE Trans. Plasma Sci. **26**, 1119 (1998).
[10] D. Wong, A. Patran, T. Tan, R. Rawat, and P. Lee, IEEE Trans. Plasma Sci. **32**, 2227 (2004).
[11] R. Petr *et al.*, Rev. Sci. Instrum. **75**, 2551 (2004).
[12] F. Beg, I. Ross, A. Lorenz, J. Worley, A. Dangor, and M. Haines, J. Appl. Phys. **88**, 3225 (2000).
[13] M. Zakaullah, K. Alamgir, M. Shafiq, M. Sharif, and A. Waheed, IEEE Trans. Plasma Sci. **30**, 2089 (2002).
[14] M. Zakaullah, K. Alamgir, M. Shafiq, M. Sharif, A. Waheed, and G. Murtaza, J. Fusion Energy **19**, 143 (2000).
[15] M. Zakaullah, K. Alamgir, M. Shafiq, S. Hassan, M. Sharif, and A. Waheed, Appl. Phys. Lett. **78**, 877 (2001).
[16] S. Hussain, M. Shafiq, R. Ahmad, A. Waheed, and M. Zakaullah, Plasma Sources Sci. Technol. **14**, 61 (2005).
[17] S. Ahmad, M. Shafiq, M. Zakaullah, and A. Waheed, Appl. Phys. Lett. **89**, 061503 (2006).
[18] C. Moreno, A. Clausse, J. Martínez, R. Llovera, and A. Tartaglione, Nukleonika **26**, 33 (2001).
[19] C. Moreno, A. Clausse, J. Martínez, R. Llovera, A. Tartaglione, M. Vénere, R. Barbuzza, and M. Del Fresno, AIP Conf. Proc. **563**, 300 (2000).
[20] C. Moreno *et al.*, Braz. J. Phys. **32**, 20 (2002).
[21] V. Raspa, L. Sigaut, R. Llovera, P. Cobelli, P. Knoblauch, R. Vieytes, A. Clausse, and C. Moreno, Braz. J. Phys. **34**, 1696 (2004).
[22] J. Mather, in *Methods of Experimental Physics*, edited by H. Lovberg and H. Griem (Academic, New York, 1971), Vol. 9 B pp. 187–249.
[23] J. Hubbell and S. Seltzer, *X-Rays Attenuation Coefficients* (NIST, Gaithersburg, 1996) http://physics.nist.gov/PhysRefData/XrayMassCoef/cover.html
[24] S. Lee, in *Small Plasma Physics Experiments II*, Proceedings of the Symposium on Small Scale Laboratory Plasma Experiments, Spring College on Plasma Physics, 1989, edited by S. Lee and P. Sakanaka (World Scientific, Singapore, 1990), pp. 113–169.